Available online at www.sciencedirect.com
SCIENCE DIRECT®
Bioorganic Chemistry 32 (2004) 244–262
BIOORGANIC CHEMISTRY
www.elsevier.com/locate/bioorg

The merits of bipartite transition-state mimics for inhibition of uracil DNA glycosylase

Yu Lin Jiang,[a] Chunyang Cao,[a] James T. Stivers,[a,*] Fenhong Song,[b] and Yoshi Ichikawa[c]

[a] *Department of Pharmacology and Molecular Sciences, The Johns Hopkins University School of Medicine, 725 North Wolfe Street, Baltimore, MD 21205-2185, USA*
[b] *Center for Advanced Research in Biotechnology of the National Institute of Standards and Technology, University of Maryland Biotechnology Institute, Rockville, MD 20850, USA*
[c] *Optimer Pharmaceuticals, Inc., 10130 Sorrento Valley Road, Suite D, San Diego, CA 92121, USA*

Received 9 January 2004
Available online 20 March 2004

Abstract

The glycosidic bond hydrolysis reaction of the enzyme uracil DNA glycosylase (UDG) occurs by a two-step mechanism involving complete bond breakage to the uracil anion leaving group in the first step, formation of a discrete glycosyl cation-uracil anion intermediate, followed by water attack in a second transition-state leading to the enzyme-bound products of uracil and abasic DNA. We have synthesized and determined the binding affinities of unimolecular mimics of the substrate and first transition-state (TS1) in which the uracil base is covalently attached to the sugar, and in addition, bimolecular mimics of the second addition transition state (TS2) in which the base and sugar are detached. We find that the bipartite mimics of TS2 are superior to the TS1 mimics. These results indicate that bipartite TS2 inhibitors could be useful for inhibition of glycosylases that proceed by stepwise reaction mechanisms.

Keywords: Uracil DNA glycosylase; 1-Azadeoxyribose; Transition-state mimics; Enzyme inhibition

* Corresponding author. Fax: 1-410-955-3023.
E-mail address: jstivers@jhmi.edu (J.T. Stivers).

0045-2068/$ - see front matter © 2004 Elsevier Inc. All rights reserved.
doi:10.1016/j.bioorg.2004.03.001

1. Introduction

As a DNA repair enzyme, uracil DNA glycosylase catalyzes the removal of uracil bases from DNA that may arise from the deamination of the normal base cytosine, or by misincorporation of dUTP into DNA during DNA replication [1]. Although the genome protective role of this enzyme is well-established, removal of uracil is also important or essential for the life cycle of several viruses, including pox-, herpes- and cytomegalo-, and thus inhibitors of the enzyme could serve as clinically useful antiviral agents [2–4]. In addition, inhibition of UDG could enhance the effectiveness of current anticancer therapies such as 5-fluorouracil and methotrexate that lead to increased accumulation of uracil in DNA [5,6]. Indeed, in yeast UDG knockout strains, high levels of uracil in DNA leads to cell cycle arrest at a G2 checkpoint [6], supporting the validity of this approach.

The mechanistic basis for the extraordinary catalytic power of UDG has been extensively investigated for the enzyme from *Escherichia coli* and humans [1]. A key insight from this work is that the enzyme facilitates a stepwise mechanism (Fig. 1A), that involves complete breakage of the *N*-glycosidic bond in the first transition state (TS1), the generation of a discrete oxacarbenium ion-uracil anion intermediate [7], followed by attack of the nucleophilic water at C1′ of the intermediate in the second transition state (TS2). Crystal structures have been obtained of a reactant analogue complex ($\mathbf{U}^{\Psi}$, Fig. 1B) [8], a bimolecular mimic of TS2 consisting of a cationic 1-aza-2′-deoxyribose (1-aza-dR) sugar and the uracil anion ($\mathbf{I} + \mathbf{U}^{-}$, Fig. 1B), and the reaction products of abasic DNA and uracil [9]. The cationic 1-aza-dR component of the TS2 mimic has been previously characterized as a tight binding ligand for the UDG–uracil anion binary complex ($K_D = 0.5\,\text{nM}$) [10]. The high affinity of this glycosyl cation mimic for the binary complex arises in large part from favorable electrostatic interactions with a conserved aspartate [11], the uracil anion [11], and anionic DNA phosphodiester groups [12]. In contrast, the very similar (but neutral) tetrahydrofuran abasic site product mimic binds weakly to the enzyme–uracil anion complex (Fig. 1B, $K_D > 15\,\mu\text{M}$) [10], establishing the importance of the sugar cation in promoting tight binding.

Although the previously characterized bipartite TS2 mimic is a potent inhibitor of UDG at pH values in which uracil component is anionic [10,11], at neutral pH values the affinity diminishes greatly, due to the unfavorable equilibrium for deprotonation of the base ($pK_a^{N1} = 9.8$) [11,13]. To address this shortcoming we have now synthesized monopartite mimics of TS1 in which the uracil base is covalently attached to the 1-azasugar in two ways (Fig. 1B), and we have also explored several low pK_a uracil analogues as improved coinhibitors with 1-aza-dR. We find that one of the new TS1 mimics has significantly greater affinity than two substrate analogues, and that the highest affinity TS2 mimic, consisting of 1-aza-dR and urazole ($pK_a = 5.8$), is superior at neutral pH to the original bipartite construct using uracil (Fig. 1B). The general merits and limitations of targeting TS1 and TS2 in stepwise glycosylase reactions are discussed.

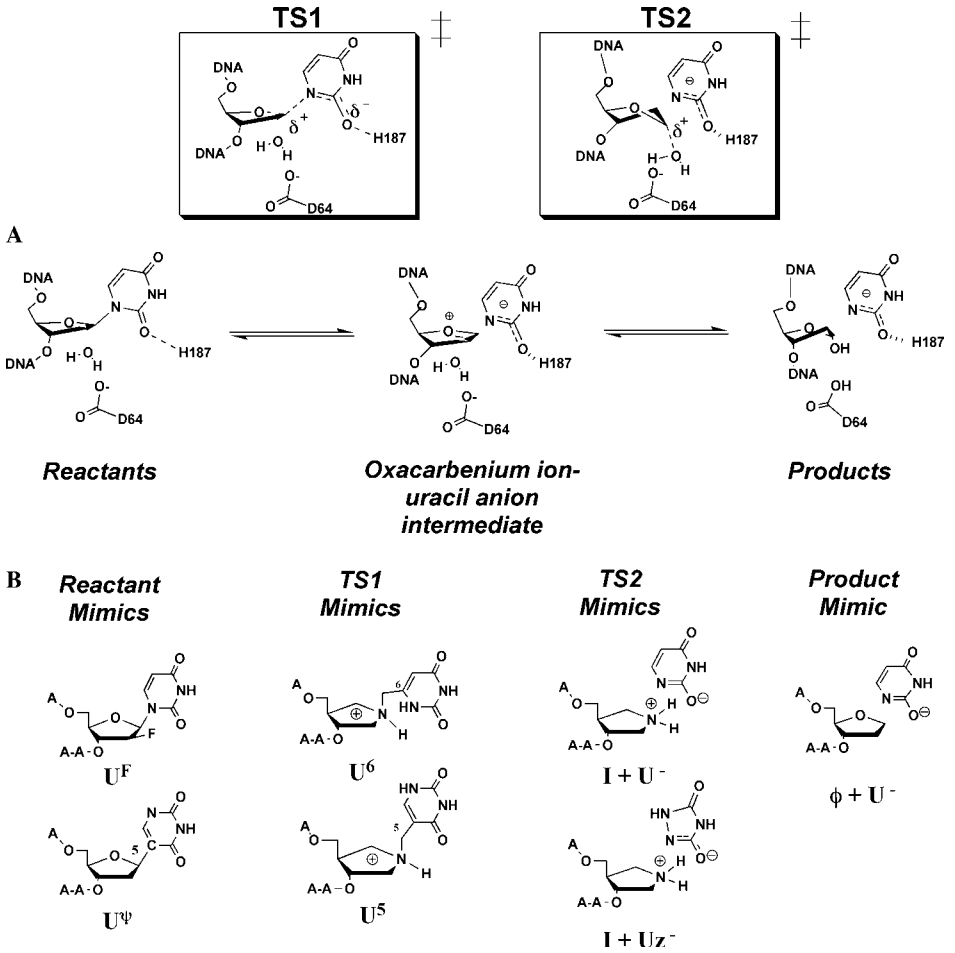

Fig. 1. The reaction coordinate of uracil DNA glycosylase (UDG) and reaction coordinate mimics. (A) UDG uses a stepwise mechanism to hydrolyze the glycosidic bond of deoxyuridine in DNA. The formation and decay of the oxacarbenium ion intermediate involves two high energy transition states (TS1 and TS2) that exhibit unique geometric and electronic features that may be mimicked by stable chemical constructs. (B) Stable chemical mimics of UDG reaction coordinate species. The 2′-fluoro-2′-deoxyuridine substrate analogue and the tetrahydrofuran abasic product analogues have been previously studied [11,15]. The other reactant and TS analogues are investigated in this work.

2. Materials and methods

2.1. Materials

As previously described, the recombinant UDG from *E. coli* strain B was purified to >99% homogeneity using a T7 polymerase-based over expression system [14]. The

concentration of the enzyme was determined using an extinction coefficient of 38.5 mM^{-1} cm^{-1}.

2.2. Phosphoramidites

All nucleoside phosphoramidites were purchased from Applied Biosystems or Glen Research (Sterling, VA), except for the 2′-β-fluoro-2′-deoxyuridine phosphoramidite which was synthesized as previously described [15], and the 1-aza-1, 2-dideoxy-4α-carba-D-ribitol 5′-trityl-3′-phosphoramidite, which was synthesized as described below.

2.3. 1-Aza-1,2-dideoxy-4α-carba-D-ribitol 5′-trityl nucleoside (2)

To a solution of **1** (0.6 g, 1.67 mmol) in CH_2Cl_2 (10 ml) [16], was added NEt_3 (0.47 ml, 3.4 mmol) and Fmoc-Cl (0.52 g, 2.0 mmol). The reaction mixture was stirred under nitrogen for 2 h, and then purified by chromatography on silica with ethyl acetate–hexanes (1:1, v/v) to give product **2** (0.78 g) in 80% yeild. ^{1}H NMR ($CDCl_3$, ppm) δ 7.77 (m, 2H); 7.58 (m, 2H); 7.43 (m, 19H); 4.37 (m, 3H); 4.22 (m, 1H); 3.62 (m, 2H); 3.25 (m, 2H); 3.10 (m, 2H); and 2.42 (m, 1H).

2.4. 1-Aza-1,2-dideoxy-4α-carba-D-ribitol 5′-trityl-3′-phosphoramidite (3)

To a solution of **2** (0.226 g, 0.39 mmol) in CH_2Cl_2 (10 ml), was added diisopropylethylamine (0.2 ml) 2-cyanoethyl diisopropylchlorophosphoramidite (130 μl, 0.57 mmol). The reaction mixture was stirred under nitrogen for 0.5 h, which was purified by chromatography on silica with ethyl acetate–hexanes–NEt_3 (1:1:0.01, v/v/v) to give product **3** (0.22 g) in 71% yield. ^{1}H NMR ($CDCl_3$, ppm) δ 7.78 (m, 2H); 7.60 (m, 2H); 7.42 (m, 19H); 4.37 (m, 3H); 4.24 (m, 1H); 3.78 (m, 3H); 3.51 (m, 3H); 3.29 (m, 1H); 3.10 (m, 3H); 2.60 (m, 3H); 1.14 (m, 12H). ^{31}P NMR ($CDCl_3$, ppm) δ 150.2 (s). ESI calc for $C_{48}H_{52}N_3NaO_5P$ (M + Na) 804, found 804. This amidite is fairy unstable in trace amounts of NEt_3, which likely catalyzes the cleavage of Fmoc group, resulting in polymerization of the amidite. Therefore, the amidite should be freshly made for DNA synthesis.

2.5. Oligonucleotide synthesis

The 4 mer oligonucleotides, $\mathbf{U^F}$, $\mathbf{U^\Psi}$, **I**, and **ϕ** (see Fig. 1B), were synthesized using standard phosphoramidite chemistry with an Applied Biosystems 390 synthesizer. In these sequences, $\mathbf{U^F}$, 2′-β-fluoro-2′-deoxyuridine nucleotide; $\mathbf{U^\Psi}$, 2′-deoxypseudouridine nucleotide; **I**, 1-aza-2-dideoxy-4α-carba-D-deoxyribonucleotide; and **ϕ**, tetrahydrofuran abasic site analogue. During synthesis of oligonucleotide containing **I**, the coupling time was increased to 10 min. In addition, the time for the trityl cleavage step was increased to 180 s instead of standard 90 s. These modifications were found to increase the incorporation efficiency at this step from 30 to 80 %. After synthesis and deprotection, the oligonucleotides were purified by anion exchange HPLC and

desalted by C-18 reversed phase HPLC (Phenomenex Aqua column). The correct size, purity, and nucleotide compositions of the final products were assessed by analytical reversed phase HPLC [Phenomenex Aqua column (250 mm × 10 mm)], MALDI mass spectrometry, and by enzymatic digestion to the constituent nucleosides (see below). The concentrations of the 4 mer oligonucleotides were determined by UV absorption measurements at 260 nm, using the pair wise extinction coefficients for the constituent nucleotides [17].

2.6. Synthesis of TS1 and TS2 mimics

As outlined in Fig. 2B, the TS1 analogues with the sequences A**U**^{6}AA and A**U**^{5}AA were synthesized by derivatizing the 1-nitrogen of A**I**AA [12], using the appropriate uracil derivative [18].

A**U**^{6}AA was prepared as follows: to dry A**I**AA (0.9 μmol), were added H_2O (10 μl), CH_3CN (30 μl), diisopropylethylamine (10 μl), and 6-chloromethyluracil (7 μl of a 29 mg/ml solution in 90:10 MeOH/diisopropylethylamine). The clear solution was stirred for 3 days at room temperature and dried in vacuo. The final product was obtained in 50% yield from the residue by HPLC using a C-18 reverse phase column. Mass (ESI) calc for MW 1181, found 1181.

A**U**^{5}AA was prepared as follows: to A**I**AA (0.2 μmol in 20 μl H_2O), were added uracil (7 μl of a 1.1 mg/ml solution H_2O) and HCHO (9 μl of a 0.28 mg/ml solution

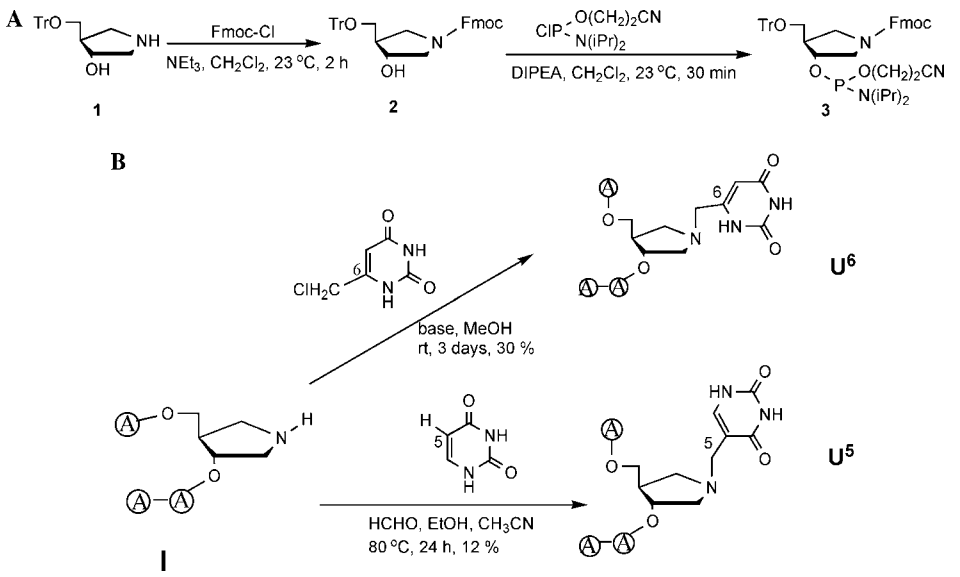

Fig. 2. Synthesis of 1-aza-deoxyribose 5′-trityl-3′-phosphoramidite (**3**) and the synthesis of TS1 mimics. (A) **3** was obtained through the sequential reaction of **1** with Fmoc-Cl and cyanoethyl-diisopropyl-chlorophosphoramidite. (B) **3** was incorporated into the DNA sequence A**3**AA (abbreviated as **I** throughout the text) using standard solid phase chemistry. **I** was used as a common synthon for the synthesis of the two TS1 analogues **U**^{5} and **U**^{6}.

in 48:48:4 EtOH/CH_3CN/NEt_3). The clear solution was then dried in vacuo. To this mixture, CH_3OH (5 μl) and CH_3CN (5 μl) were added. The resulting mixture was sealed and incubated at 80–85 °C for 24 h and dried in vacuo. The final product was obtained in 12% yield from the residue by HPLC using a C-18 reverse phase column. Mass (ESI) calc for MW 1181, found 1181.

2.7. Nucleotide composition analysis

The nucleotide compositions of A**U**^{5}AA and A**U**^{6}AA were confirmed by digestion with P1 nuclease and alkaline phosphatase (both obtained from Roche Diagnostics) followed by separation of the constituent nucleosides using reversed phase HPLC (Phenomenex C-18 Aqua column, 5 mm × 250 mm) with monitoring at 260 nm and isocratic elution (7% CH_3CN, 0.1 M TEAA, pH 7.0). The identity of the peaks was confirmed by comparison with the retention times of authentic nucleoside standards and the ratio of the peak areas were consistent with the expected stoichiometries and extinction coefficients of these tetramers. The standards for the 2′-deoxynucleoside forms of **U**^{5} and **U**^{6} were synthesized as previously described [18]. The structures of the deoxynucleoside standards were ascertained by ^{1}H-NMR spectroscopy and ESI–MS analyses.

2.8. Competitive inhibition measurements

For measuring the binding of the single stranded 4 mer **U**^{F} substrate and **ϕ** product analogue DNA to the free enzyme, competitive kinetic inhibition measurements were performed using the substrate Ap**U**pAp [19]. Conditions were chosen whereby $[UDG]_{tot} \ll$ [inhibitor] or [Ap**U**pAp], and [Ap**U**pAp] $\ll K_m$. Accordingly, K_i could be obtained directly from a plot of k/k_0 against [inhibitor] as shown in Eq. (1), where k is the observed rate constant ($v/[UDG]_{tot}$) at a given [inhibitor], and k_0 is the observed rate constant in the absence of the inhibitor:

$$k/k_0 = 1/(1 + [X]/K_i). \quad (1)$$

For these measurements, a sensitive HPLC kinetic assay for monitoring the formation of the abasic product was employed [20]. All experiments were performed at 25 °C using TMN buffer at pH 8 (10 mM Tris–HCl, 2.5 mM $MgCl_2$, and 25 mM NaCl). For determination of the dissociation constants of the uracil analogues in Table 1, an alternative fluorescence-based competitive inhibition kinetic assay was used [10].

2.9. Binding of 1-aza-dR to the UDG binary complex

The dissociation constants for binding of **I** to the UDG–uracil or UDG–urazole complex were determined by competition binding measurements in which a 2-aminopurine (2AP) labeled abasic analogue DNA (**ϕ19**) was displaced from the EU or EUz binary complex as previously described [10]. The sequence of **ϕ19** has been previously reported [21], and this DNA construct shows a strong fluorescence decrease when it binds to the EU binary complex that can be used as a spectroscopic signal in

competition binding measurements. Measurements were performed at 25 °C in TMN buffer at pH 7 and 8. Before performing the competition binding experiments, the K_D values of **ϕ19** for the EU and EUz complexes were determined at pH 8 and 7 using direct binding measurements. In these measurements, the decrease in 2AP fluorescence was followed upon titrating a solution containing 200 nM **ϕ19** and 1 mM uracil (or urazole) with increasing concentrations of UDG. This concentration of uracil (or urazole) is over 10-fold greater than the apparent K_D of uracil or urazole for the enzyme. This insures that UDG is saturated with either base, and that the measurements reflect binding of **ϕ19** to the enzyme–base binary complex. Excitation was at 320 nm and emission spectra from 340 to 450 nm were collected using a Spex Fluoromax 3 spectrofluorimeter. The fluorescence intensity (F) at 370 nm was plotted against $[EU]_{tot}$, or $[EUz]_{tot}$ to obtain the K_D from Eq. (2), where $[X]_{tot}$ represents either $[EU]_{tot}$ or $[EUz]_{tot}$.

$$F = F_0 - \{(F_0 - F_f)[\boldsymbol{\phi 19}]_{tot}/2\}\{b - (b^2 - 4[X]_{tot}[\boldsymbol{\phi 19}]_{tot})^{1/2}\}, \quad (2)$$

$$b = K_D + [X]_{tot} + [\boldsymbol{\phi 19}]_{tot}.$$

To determine the affinity of **I** for the EU and EUz binary complexes, titrations included a saturating concentration of uracil (1 mM) so that at the beginning of the titration UDG was completely bound as E · U or E · U · **ϕ19**. The concentrations of **ϕ19** and UDG in the individual experiments are reported in the legends to Figs. 4 and 8. The dissociation constants of **I** for the EU or EUz complex ($K_D^{I,EU}$) were then determined using the computer program *Dynafit* [22] and the equilibria shown in Eqs. (3) and (4), employing the known dissociation constants of **ϕ19** for the EU and EUz complexes as determined from Eq. (2) above:

$$E \cdot \mathbf{U} \cdot \boldsymbol{\phi 19} \overset{K_D^{\phi,EU}}{\rightleftharpoons} E \cdot \mathbf{U} + \boldsymbol{\phi 19} \quad (3)$$

$$E \cdot U \cdot \mathbf{I} \overset{K_D^{I,EU}}{\rightleftharpoons} E \cdot U + \mathbf{I} \quad (4)$$

2.10. ^1H NMR spectroscopy

Samples (0.5 ml in 90% H_2O and 10% D_2O for frequency lock) contained 0.3 mM UDG, 2 mM uracil, 5-azauracil or urazole, 10 mM NaH_2PO_4 (pH 7.5 or 9), and 150 mM NaCl. The samples were placed in 5 mm NMR tubes (Wilmad 535-PP, Buena, NJ) and sealed with parafilm. The experiments were collected at 25 °C on a Varian INOVA 500 MHz spectrometer using a binomial 1-5-10-5-1 pulse sequence that minimizes excitation of water [23]. Acquisition and processing parameters were: 2k complex points, 68 ms acquisition time, and 15 Hz line broadening.

2.11. Computational modeling

The structural models and electrostatic potential surfaces shown in Fig. 9 were obtained with the program Spartan Pro (Wavefunction) using semi-empirical meth-

ods (HF/AM1). The truncated models included all atoms of the base and sugar, but the 5′ and 3′ phosphodiester groups were omitted and replaced with hydrogen atoms. The reactant structure was obtained directly from the coordinates of pdb deposition 1EMH without any further optimization before calculating the electrostatic potential surface. The TS1 model was obtained by constraining the sugar in a 3′-exo conformation calculated from KIE measurements [7], and orienting the base in the position observed in the structure of uracil and 1-aza-dR (1QF3), except that the N1 nitrogen was moved to a distance of 2.75 Å from the anomeric carbon, which corresponds to a dissociative transition state with less than 0.01 bond order to the leaving group [24]. The model for TS2 was obtained directly from the structure of uracil and 1-aza-dR (1QF3) by substituting a carbon atom for the 1-NH_2^+ of the sugar. The geometry optimized structures and electrostatic potential surfaces for $\mathbf{U^5}$ and $\mathbf{U^6}$ in Fig. 9B were calculated using semi-empirical methods (HF/AM1), and were manually superimposed with the structural models for TS1. The model for bound urazole and 1-aza-dR in Fig. 9C was obtained from 1QF3 by substituting the appropriate atoms of the uracil base, followed by constrained energy minimization.

3. Results

3.1. Synthesis of novel TS1 analogues

The characteristics of TS1 are an elongated glycosidic bond, a significant positive charge development on the sugar, and negative charge development on the uracil leaving group (Fig. 1A). To imitate these attributes, we synthesized the two TS1 mimics shown in Fig. 1B. The first mimic ($\mathbf{U^6}$), has the 1-nitrogen linked to the uracil base at the 6-position through a methylene bridge. This analogue was anticipated to imitate the elongated glycosidic bond and the developing positive charge on the sugar in a dissociative transition state. In addition, since the glycosidic nitrogen of the uracil base of $\mathbf{U^6}$ is not involved in a covalent bond to the sugar, it is free to lose a proton and generate an anion in the active site, as previously observed for uracil [13,25]. This anion would be anticipated to provide stabilization to the glycosyl cation [11]. The second TS1 mimic ($\mathbf{U^5}$), is similar to $\mathbf{U^6}$ in that a methylene bridge connects the sugar and base (Fig. 1B). However, the bridge connects to the 5-position of the uracil, and therefore, the orientation of the base heteroatoms differs from $\mathbf{U^6}$. In addition, the N1-nitrogen of $\mathbf{U^5}$ is not positioned as close to the sugar as $\mathbf{U^6}$, and therefore this position may not ionize and provide stabilization to the glycosyl cation.

The TS1 analogues shown in Fig. 1B were all synthesized from a common 4 mer oligonucleotide precursor (**I**) that contained the 1-azadeoxyribose moiety (Figs. 1A and B). Although UDG does bind more tightly to longer oligonucleotides [10,20], the 4 mer has been shown to possess all of the binding determinants required for tight binding of the 1-aza-dR group [10,12,19]. The 4 mer was prepared using standard solid phase phosphoramidite DNA chemistry using the commercially available adenosine nucleotide 3′-phosphoramidite, and the custom made 1-aza-1,2-dideoxy-4α-carba-D-ribitol 5′-trityl-3′-phosphoramidite (**3**, Fig. 1A) [10,16].

Once the **I** synthon was in hand (Fig. 1B), it was fairly straight forward to derivatize its 1-nitrogen with 6-chloromethyluracil or uracil in the presence of formaldehyde to yield the $\mathbf{U}^{6}$ and $\mathbf{U}^{5}$ TS1 analogues shown in Fig. 2. These syntheses are similar to those used previously to obtain analogous 1-aza-uridine nucleosides [26], but this report is the first to generate these nucleotides in a DNA scaffold. Although the yields are only in the range 12–30%, and the crude reaction products required purification by high-performance liquid chromatography, sufficient material was obtained to perform a large number of biochemical experiments.

3.2. Relative binding affinities of substrate, TS1, and bipartite TS2 analogues

Two substrate analogues, $\mathbf{U}^{\Psi}$ and $\mathbf{U}^{\mathbf{F}}$, were constructed for binding affinity comparisons with the TS1 and TS2 analogues described below (Fig. 1B). Dissociation constants for the substrate and TS1 mimics were determined by a competitive inhibition kinetic assay as previously described (Fig. 3) [12]. $\mathbf{U}^{\Psi}$ and $\mathbf{U}^{\mathbf{F}}$ were found to bind with similar affinities of 5.5 and 4.8 μM, respectively, while the TS1 mimic $\mathbf{U}^{5}$ bound 10 to 12-fold more tightly ($K_D = 0.5 \pm 0.04\,\mu M$). The other TS1 mimic, $\mathbf{U}^{6}$, was found to bind with similar affinity as the two substrate mimics ($K_D = 4.8 \pm 0.5\,\mu M$), indicating that linking uracil via a methylene bridge to the 6-position is less effective than to the 5-carbon (i.e., $\mathbf{U}^{5}$). These results suggest that $\mathbf{U}^{5}$ captures some of the electronic and geometric features of TS1.

An assumption in ascribing the enhanced binding affinity of $\mathbf{U}^{5}$ to mimicry of TS1 is that the 1-nitrogen of the sugar is protonated. Previous NMR and pH studies have established that the pK_a for free 1-aza-dR is 9.5, and that its nitrogen is protonated when bound to the EU^{-} complex in the pH range 7–9 [11]. Because direct measurement of the 1-nitrogen pK_a values in the context of $\mathbf{U}^{5}$ by NMR spectroscopy is not trivial, and we examined binding of $\mathbf{U}^{5}$ at pH 6.5 to assess whether the measurements at pH 8 involved the neutral 1-azasugar. In contrast with the anticipated increase in binding affinity if protonation of the sugar occurred as the pH was lowered from 8.0

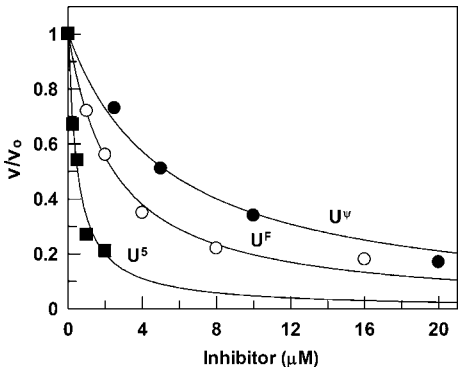

Fig. 3. Inhibition of UDG by the substrate analogues $\mathbf{U}^{\Psi}$, $\mathbf{U}^{\mathbf{F}}$, and the TS1 analogue $\mathbf{U}^{5}$. A competitive kinetic inhibition assay was used. The curves are nonlinear best fits to Eq. (1).

to 6.5, $\mathbf{U}^5$ bound more weakly at pH 6.5, with $K_D = 8.3\,\mu M$. The weaker binding at pH 6.5 may be partially attributed to protonation of the catalytic aspartate (pK_a 6.5) that is positioned below the α face of the sugar (Fig. 1A) [9,27].

The salient features of TS2 are the lack of covalent bonding between the sugar and the anionic uracil, and significant positive charge at C1′ (Fig. 1). Thus a good mimic of TS2 is the bipartite combination of uracil and **I** (Fig. 1B). Binding of **I** to EU^- complex can be followed by competitively displacing a fluorescent abasic DNA analogue (ϕ, Fig. 4) [10], and is pH dependent because interaction of this glycosyl cation mimic is enhanced by the negative charge on the bound uracil base ($pK_a^{EU} = 7.5$) [25]. As previously shown, **I** binds very tightly at pH 8.0 with a $K_D = (5 \pm 0.4) \times 10^{-4}\,\mu M$ (solid curve, Fig. 4) [10]. However at pH 7, where the bound uracil is 75% neutral, **I** binds 300-fold more weakly ($K_D = 0.14 \pm 0.03\,\mu M$). A bar chart is shown in Fig. 5 that compares the relative affinities of the substrate and TS1 mimics at pH 8.0, and the TS2 mimic at pH 8.0 and 7.0. Although this comparison clearly reveals that the bipartite TS2 mimic ($\mathbf{I} + \mathbf{U}^-$) is superior at pH 8.0, the Achilles' heel of this mimic is that the pK_a values for the free and bound uracil are too high to generate the required anionic form at neutral pH, leading to weak binding of both **U** and **I** under physiological conditions. A further discussion of the merits and limitations of TS2 mimicry is presented later.

3.3. Screening low pK_a uracil analogues for improved coinhibitors

One strategy to improve the potency of the TS2 mimic at a physiological pH value is to find uracil analogues that have decreased pK_a values as compared to uracil itself

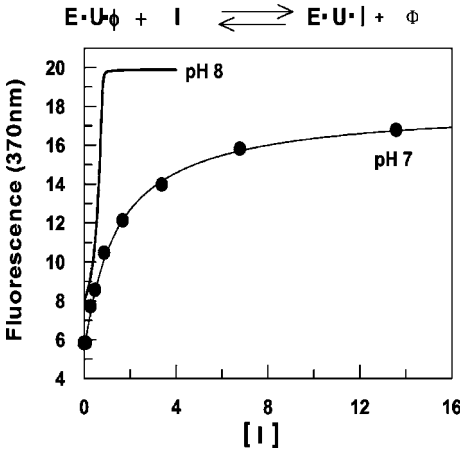

Fig. 4. pH dependence of **I** binding to the EU complex. A competitive displacement assay was used in which a fluorescent abasic site analogue (ϕ) was dissociated from the EU complex upon binding of **I** [10]. The solid curve shows the previously obtained fitted curve for binding of **I** to the EU complex at pH 8 [10]. The measurements at pH 7 used 1 mM uracil, 330 nM UDG, and 200 nM ϕ. The curve was calculated using the program *Dynafit* [22].

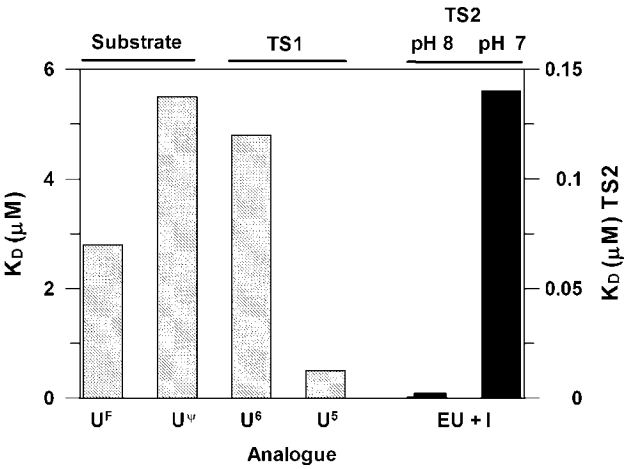

Fig. 5. Relative K_D values (μM) of substrate and TS1 analogues at pH 8.0 (left graph axis), and the bipartite TS2 mimic at pH 8.0 and 7.0 (right graph axis).

($pK_a(N1)^{free} = 9.8$, $pK_a(N1)^{bound} = 6.4$) [13]. With this aim, we screened six uracil analogues with pK_a values ranging from 5.8 to 8 for their ability to competitively inhibit the reaction of UDG at pH 8 and 7 (Table 1). As a point of reference, uracil binds 8.2-fold more weakly as the pH is lowered in this range, due to protonation of the bound uracil [25]. Most of the uracil analogues in Table 1 with $pK_a(N1)^{free}$ values of 6.7–8.0 show 1.5- to 5.9-fold weaker binding as the pH was lowered from 8 to 7, which arises from protonation of both the bound and free uracil. The magnitude of the binding decrement parallels the proton affinities of these analogues (Table 1), but it is impossible to be more quantitative about the trends because the pK_a values for the bound uracil analogues are not known. One analogue, urazole ($pK_a = 5.8$), showed pH independent binding over the pH range investigated (Fig. 6), and furthermore, bound 14-fold more tightly than uracil at pH 7 ($K_D = 98\ \mu M$) (Fig. 6B, Table 1).

Table 1
pK_a values and dissociation constants for uracil analogues[a]

	pK_a	K_d (mM)		K^8/K^{7b}
		pH 8	pH 7	
U	9.8	0.17 ± 0.02	1.4 ± 0.1	0.12
5-FU	8.0	6.2 ± 1.2	9.6 ± 1.6	0.65
6-AU	7.6	0.39 ± 0.01	1.4 ± 0.1	0.27
6-CF3-U	7.4	0.11 ± 0.01	0.30 ± 0.03	0.37
CA	7.2	0.098 ± 0.016	0.58 ± 0.11	0.17
5-AU	6.7	0.43 ± 0.04	0.98 ± 0.02	0.44
Uz	5.8	0.092 ± 0.008	0.098 ± 0.004	0.94

[a] The pK_a values for U, 5-FU, 6-AU, 6-CF_3-U, CA, 5-AU, and Uz were obtained from [46–52], respectively.

[b] The ratio of the dissociation constants at pH 8 and 7.

Because urazole showed favorable binding properties to the free enzyme, we investigated its binding interactions in more detail using NMR spectroscopy. Previous NMR studies of uracil binding to UDG have revealed the presence of a very downfield shifted proton resonance that arises from a hydrogen bond between uracil O2 and the imidazole NH of His187 in the active site (Fig. 1A) [11,13,28]. This hydrogen bond stabilizes the uracil anion in the active site by 5 kcal/mol and plays an indirect but essential role in binding of **I** by facilitating formation of the uracil anion component of the electrostatic sandwich that cradles the sugar cation [11]. To directly test whether the urazole anion persists at neutral pH in the UDG active site, we collected NMR spectra of UDG in the presence of uracil, 5-azauracil, and urazole at pH 9.0 and 7.5 (Figs. 7A and B). At pH 9.0, uracil and urazole both show the expected resonance at 14.6 and 14.8 ppm, but 5-azauracil does not. The absence of the proton resonance for 5-azauracil is consistent with its weaker binding to the enzyme, and suggests that this may be due to its improper positioning in the active site. When the pH is lowered to 7.5, only the downfield resonance of urazole remains, while that for uracil is broadened beyond the limits of detection. This NMR result strongly supports the proposal that the pH independent binding of urazole, and its enhanced

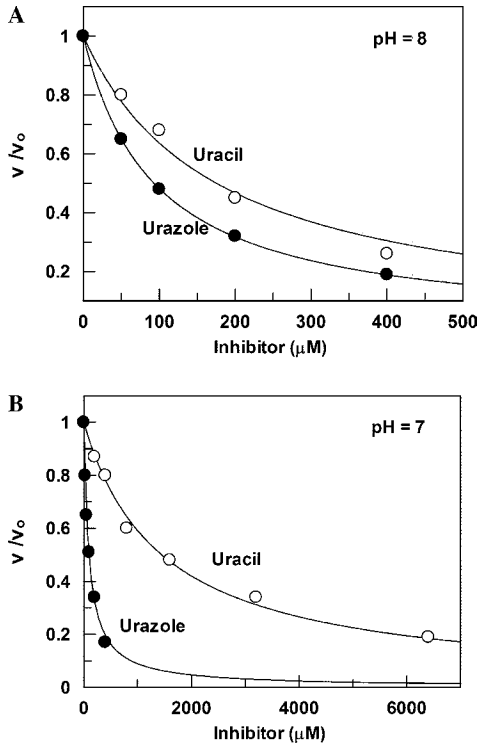

Fig. 6. Competitive inhibition of the reaction of UDG with the substrate **AU**Ap (1 μM) by uracil and urazole at (A) pH 8 and (B) pH 7.

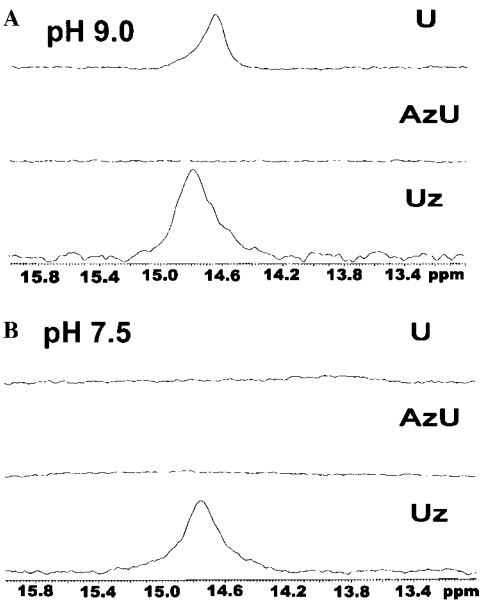

Fig. 7. ^{1}H NMR spectra of uracil (U), 5-azauracil (AzU), and urazole (Uz) bound to UDG at (A) pH 9.0 and (B) pH 7.5. The downfield resonance arises from the interaction of the $N^{\varepsilon H}$ of His187 with the O2 anion of U and Uz (see text).

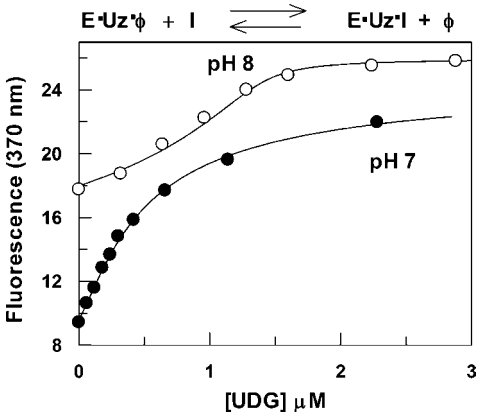

Fig. 8. Binding of **I** to the EUz complex at pH 8 and 7. The measurements at pH 8 used 1.4 μM UDG, 200 nM ϕ, and 1 mM urazole (Uz). The measurements at pH 7 used 330 nM UDG, 200 nM ϕ, and 1 mM urazole (Uz). The curves were calculated with the program *Dynafit* [22].

affinity as compared to uracil, arises from its reduced pK_a, allowing it to be negatively charged at neutral pH.

Because of the enhanced binding of urazole at neutral pH, we investigated this analogue as a coinhibitor with **I** (Fig. 8). Using the competitive displacement fluorescence assay, **I** was found to bind to the EUz^{-} complex with an affinity of

14 ± 4 and 49 ± 5 nM at pH 8 and 7, respectively. Thus at a physiological pH 7.4, **I** binds to the EUz^- complex with an affinity of about 30 nM as estimated from interpolation between these measured values. This affinity is 170-fold greater than the substrate analogues bind to the free enzyme.

4. Discussion

4.1. Targeting TS1 in stepwise glycosylase reactions

Glycosylase reactions have long been amenable to the design of inhibitors that mimic features of high energy structures along the reaction coordinate, thereby capturing a portion of the enzyme's strong binding energy for these species [29–35]. In the case of a stepwise glycosylase reaction, where a discrete oxacarbenium ion

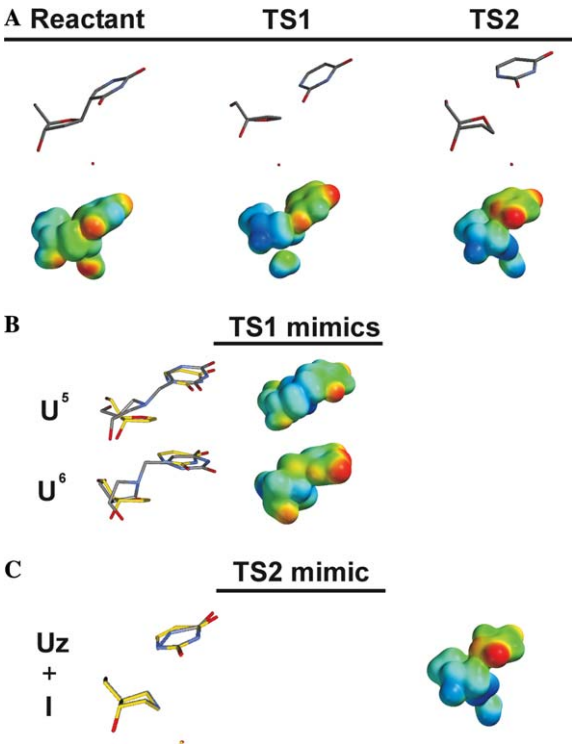

Fig. 9. Structural and electrostatic potential models for reactant, TS1, TS2, and chemical mimics. (A) Structural models for the bound substrate analogue $\mathbf{U}^{\Psi}$ and the two transition states of the stepwise reaction catalyzed by UDG. (B) Geometry optimized structural models for $\mathbf{U}^{5}$ and $\mathbf{U}^{6}$ superimposed on the model for TS1. The electrostatic potentials are plotted on the van der Waals surfaces, which are shown to the right of each model. (C) Geometry optimized structural model for the bipartite TS2 mimic of urazole and **I** superimposed on the model for TS2. The electrostatic potential surface of $\mathbf{Uz} + \mathbf{I}$ is shown to the right. The details of how these models were calculated are described in Section 2.

intermediate is formed, it is possible to envision the design of molecules that mimic TS1, the intermediate, or TS2. In general, which of these mimics becomes the most useful inhibitor will depend on how closely the unique charge and geometric properties of these reaction coordinate species are reproduced by the inhibitor. In addition, to become useful inhibitors, bipartite intermediate and TS2 mimics must also possess sufficient binding energy to overcome the unfavorable entropic penalties associated with binding of the two molecular components from solution. A transition state mimicry strategy employing both 1′ and 4′-azasugars has been used previously to potently inhibit several DNA glycosylases [36,37].

Mimics of TS1 in which the sugar and base are covalently tethered must reproduce the elongated bond lengths of this dissociative transition state [24,38], as well as the charge distributions on the sugar and base. In addition, the linker must allow favorable positioning of the leaving group and sugar relative to enzyme groups that form stabilizing interactions with these parts of the substrate. Using the classic pseudo-thermodynamic framework developed by Radzicka and Wolfenden [39], the maximum binding affinity for a perfect TS1 mimic would be equal to $K_D = k_{non}/(k_{cat}/K_m)$, where k_{non} is the rate of the uncatalyzed glycosidic bond cleavage reaction. In the case of UDG and its substrate **A**U**A**A, $k_{non}/(k_{cat}/K_m) = 10^{-10}\,s^{-1}/(3 \times 10^6\,M^{-1}\,s^{-1}) \sim 10^{-17}\,M$ [1,10]. Accordingly, a perfect TS1 mimic would be expected to bind almost twelve-orders of magnitude more tightly than the $\mathbf{U}^{\Psi}$ and $\mathbf{U}^{\mathbf{F}}$ substrate analogues (Fig. 1B). Although the TS1 mimics studied here bind as much as 12-fold more tightly than the substrate analogues, they capture only a tiny fraction of the theoretical interaction energy expected from a perfect TS1 mimic.

Previous structural and mechanistic studies provide an informative basis for understanding the comparatively weak binding affinity of the TS1 mimics. In the crystal structure of UDG bound to DNA containing the substrate analogue deoxypseudouridine ($\mathbf{U}^{\Psi}$), the nucleotide base and sugar are oriented in a highly distorted conformation in which the base is nearly coplanar with the sugar ring, and the C–C glycosidic bond is elongated (1.55 Å, Fig. 9A) [8]. This ground-state conformation appears to be significantly strained, and likely represents a high energy conformation approaching that of TS1, which is highly dissociative [7]. A reasonable structural model for TS1 is shown in Fig. 9A, which was obtained from three pieces of information (see Section 2): (i) the crystallographic coordinates of $\mathbf{U}^{\Psi}$ [8], (ii) the results from KIE studies that provide the sugar pucker and C1′–N1 bond order in TS1 (<0.01) [7], and the position of the uracil base in the crystal structure of the bipartite TS2 mimic of uracil and 1-aza-dR [40]. A model of TS1 obtained using this information is superimposed with energy minimized models of $\mathbf{U}^{6}$ and $\mathbf{U}^{5}$ in Fig. 9B. As compared to the glycosidic bond of the substrate analogue $\mathbf{U}^{\Psi}$, the methylene bridges of $\mathbf{U}^{6}$ and $\mathbf{U}^{5}$ increase the linear distance between the base and sugar from 1.55 to about 2.6 Å. However as shown in Fig. 9B, the constraints imposed by the methylene bridge groups do not allow an orientation of the base and sugar that precisely mimics that of TS1.

In addition to the relatively poor structural mimicry by $\mathbf{U}^{6}$ and $\mathbf{U}^{5}$, these analogues also poorly match the charge distribution on the sugar and base in TS1. This can be appreciated from comparison of the electrostatic potential surfaces of

these TS1 mimics with that of the TS1 model (Figs. 9A and B). For instance, $\mathbf{U}^5$ and $\mathbf{U}^6$ both mimic the positive charge character at C1′, but they poorly match the negative potential on the uracil leaving group, because the electrons of their intact glycosidic bonds are not able to delocalize onto the O2 atom of the base. A potent purine based TS1 inhibitor (**4**) analogous to $\mathbf{U}^5$ and $\mathbf{U}^6$ has been synthesized for the enzyme purine nucleoside phosphorylase (PNP) from bovine and *Mycobacterium tuberculosis* (Mt) [34,41].

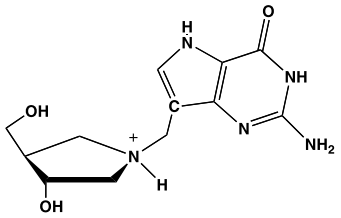

4

The MtPNP follows a dissociative but concerted mechanism and the methylene bridge analogue (**4**) presumably mimics the features of this transition-state ($K_D = 24$ pM) [34]. In contrast, the bovine PNP shows an earlier more associative transition-state, and accordingly, (**4**) bound much more weakly [34,42]. For UDG, neither type of TS1 inhibitor is very effective because of the highly unusual orientation of the sugar and base, and the optimization of the active site towards stabilization of the electronic features of the oxacarbenium ion intermediate and TS2.

4.2. The merits of targeting TS2

The properties of TS2 are a fully dissociated uracil base, which has accumulated a full negative charge, and a glycosyl cation that will have developed some bonding to the incoming water nucleophile. The recent crystal structure of **I** and the uracil anion bound to human UDG shows that **I** assumes a distorted conformation in which the imino nitrogen is displaced from the plane of the sugar ring towards the attacking water [40]. An implication of this structure is that the planar conformation of the oxacarbenium ion intermediate is broken in TS2, and that the electrophilic anomeric carbon migrates to meet the water nucleophile. Thus, although **I** was originally thought to mimic the planar oxacarbenium ion intermediate, its nonplanar conformation, and its charge localization on the 1′ position, makes it a much better mimic of TS2. The structure and corresponding electrostatic model of the bipartite TS2 mimic consisting of urazole and **I** is shown in Fig. 9 for comparison with a model of TS2 (Fig. 9A), which was constructed from the crystallographic coordinates of 1Q3F. The excellent geometric and electrostatic match between the bipartite inhibitor and TS2 is much better than that observed for any of the TS1 mimics (see above).

The development of bipartite TS2 inhibitors for glycosylase reactions is a nontraditional approach, because a single substrate molecule is deconstructed into two

parts, each of which mimics the presumed features of a bimolecular transition state. This contrasts with the bisubstrate analogue strategy, where two reactants are covalently tethered to capture the binding energy of the two halves, thereby bypassing the entropic penalty for binding two molecules from solution [43,44]. The inherent difficulty with this bimolecular approach is that the binding of each component is comparatively weak in the absence of the other component. Thus in general, the individual binding energy of at least one of the parts must be sufficiently large to significantly populate the enzyme under physiological conditions. Under such conditions, binding of the first component creates the binding environment that allows tight binding of the second component, and creation of the high affinity bimolecular inhibitor complex. In practical terms, this requires that the intracellular concentration of at least one of the component parts be high relative to its K_D. Of course, a monopartite TS2 mimic could provide a significant entropic advantage over the bipartite mimic if the correct structural features could be captured.

In principle, the above thermodynamic problem for a bipartite inhibitor may be overcome if one of the components is also the last reaction product to be released (such as the uracil anion in this case) [10]. For such an ordered product release mechanism, the second component (1-aza-dR in this case) will bind avidly to the enzyme–product complex, and the inhibition mechanism will be noncompetitive with respect to substrate. For UDG, in vitro studies at pH 8.0 have shown that 80 nM **I** provided 95% inhibition of UDG in the absence of any added uracil coinhibitor, and that this strong inhibition arose from **I** binding tightly to the EU product complex [10]. Of course, both U and **I** also bind to the free enzyme, but these inhibition pathways will not be significant given the weak affinities of the individual parts for the free enzyme at physiological pH. A noncompetitive mode of inhibition is especially advantageous for targeting a DNA repair enzyme that not only binds to damaged target sites in DNA, but also binds nonspecifically to nontarget DNA, which is present at high concentrations in cells.

5. Conclusion

We have explored chemical analogues that mimic the features of several species along the stepwise enzymatic reaction coordinate of UDG. In general, these findings show that bipartite TS2 mimics can serve as effective inhibitors for glycosylase reactions that proceed by stepwise mechanisms. In favorable cases, the bipartite approach can offer advantages over unimolecular TS1 inhibitors because stable chemical analogues of TS2 may be better able to match the geometries and charge distributions of the cationic sugar and leaving group. Furthermore, we suggest that this strategy is likely to be most successful when the following conditions are met: (i) when one of the inhibitor components is the anionic product leaving group of the reaction, (ii) when the free and bound forms of the leaving group product have the correct anionic ionization state at physiological pH, and (iii) when the intracellular concentration of the leaving group product is comparable to or greater than its K_D. In addition, the inhibition is noncompetitive with respect to substrate, which is

desirable when high concentrations of substrate are present in the cellular environment. Several reactions that potentially meet these criteria are those catalyzed by sugar-NDP hydrolases or transferases [32,45], nucleoside phosphorylases [42], and phosphoribosyl transferases [42].

Acknowledgments

This work was supported by National Institutes of Health Grant GM46835 (J.T.S.), and by the DOD Breast Cancer Research Program DAMD17-03-1-1251.

References

[1] J.T. Stivers, Y.L. Jiang, Chem. Rev. 103 (2003) 2729–2759.
[2] R. Chen, H. Wang, L.M. Mansky, J. Gen. Virol. 83 (2002) 2339–2345.
[3] A.K. Millns, M.S. Carpenter, A.M. DeLange, Virology 198 (1994) 504–513.
[4] R.B. Pyles, R.L. Thompson, J. Virol. 68 (1994) 4963–4972.
[5] R.D. Ladner, Curr. Protein Pept. Sci. 2 (2001) 361–370.
[6] B.A. Tinkelenberg, M.J. Hansbury, R.D. Ladner, Cancer Res. 62 (2002) 4909–4915.
[7] R.M. Werner, J.T. Stivers, Biochemistry 39 (2000) 14054–14064.
[8] S.S. Parikh, G. Walcher, G.D. Jones, G. Slupphaug, H.E. Krokan, G.M. Blackburn, J.A. Tainer, Proc. Natl. Acad. Sci. USA 97 (2000) 5083–5088.
[9] S.S. Parikh, C.D. Mol, G. Slupphaug, S. Bharati, H.E. Krokan, J.A. Tainer, EMBO J. 17 (1998) 5214–5226.
[10] Y.L. Jiang, Y. Ichikawa, J.T. Stivers, Biochemistry 41 (2002) 7116–7124.
[11] Y.L. Jiang, A.C. Drohat, Y. Ichikawa, J.T. Stivers, J. Biol. Chem. 277 (2002) 15385–15392.
[12] Y.L. Jiang, Y. Ichikawa, F. Song, J.T. Stivers, Biochemistry 42 (2003) 1922–1929.
[13] A.C. Drohat, J.T. Stivers, J. Am. Chem. Soc. (2000) 1840–1841.
[14] A.C. Drohat, G. Xiao, M. Tordova, J. Jagadeesh, K.W. Pankiewicz, K.A. Watanabe, G.L. Gilliland, J.T. Stivers, Biochemistry 38 (1999) 11876–11886.
[15] J.T. Stivers, K.W. Pankiewicz, K.A. Watanabe, Biochemistry 38 (1999) 952–963.
[16] K. Makino, Y. Ichikawa, Tetrahedron Lett. 39 (1998) 8245–8248.
[17] G.D. Fasman, Handbook of Biochemistry and Molecular Biology: Nucleic Acids, third ed., vol. 1, CRC Press, Boca Raton, FL, 1975.
[18] V.V. Filichev, E.B. Pedersen, Tetrahedron 57 (2001) 9163–9168.
[19] Y.L. Jiang, J.T. Stivers, Biochemistry 40 (2001) 7710–7719.
[20] Y.L. Jiang, K. Kwon, J.T. Stivers, J. Biol. Chem. 276 (2001) 42347–42354.
[21] J.T. Stivers, Nucleic Acids Res. 26 (1998) 3837–3844.
[22] P. Kuzmic, Anal. Biochem. 237 (1996) 260–273.
[23] P.J. Hore, J. Magn. Reson. 61 (1983) 567–570.
[24] V.L. Schramm, Curr. Opin. Chem. Biol. 5 (2001) 556–564.
[25] A.C. Drohat, J.T. Stivers, Biochemistry 39 (2000) 11865–11875.
[26] S.U. Hansen, M. Bols, Acta Chem. Scand. 52 (1998) 1214–1222.
[27] A.C. Drohat, J. Jagadeesh, E. Ferguson, J.T. Stivers, Biochemistry 38 (1999) 11866–11875.
[28] J. Dong, A.C. Drohat, J.T. Stivers, K.W. Pankiewicz, P.R. Carey, Biochemistry 39 (2000).
[29] A. Bulow, I.W. Plesner, M. Bols, Biochim. Biophys. Acta 1545 (2001) 207–215.
[30] H. Liu, X. Liang, H. Sohoel, A. Bulow, M. Bols, J. Am. Chem. Soc. 123 (2001) 5116–5117.
[31] B.L. Mark, D.J. Vocadlo, D. Zhao, S. Knapp, S.G. Withers, M.N. James, J. Biol. Chem. 276 (2001) 42131–42137.
[32] L. Qiao, B.W. Murray, M. Shimazaki, J. Schultz, C.-H. Wong, J. Am. Chem. Soc. 118 (1996) 7653–7662.

[33] G.A. Kicska, L. Long, H. Horig, C. Fairchild, P.C. Tyler, R.H. Furneaux, V.L. Schramm, H.L. Kaufman, Proc. Natl. Acad. Sci. USA 98 (2001) 4593–4598.
[34] A. Lewandowicz, W. Shi, G.B. Evans, P.C. Tyler, R.H. Furneaux, L.A. Basso, D.S. Santos, S.C. Almo, V.L. Schramm, Biochemistry 42 (2003) 6057–6066.
[35] A. Lewandowicz, P.C. Tyler, G.B. Evans, R.H. Furneaux, V.L. Schramm, J. Biol. Chem., 2003.
[36] L. Deng, O.D. Schaerer, G.L. Verdine, J. Am. Chem. Soc. 119 (1997) 7865–7866.
[37] O.D. Scharer, H.M. Nash, J. Jiricny, J. Laval, G.L. Verdine, J. Biol. Chem. 273 (1998) 8592–8597.
[38] V.L. Schramm, W. Shi, Curr. Opin. Struct. Biol. 11 (2001) 657–665.
[39] A. Radzicka, R. Wolfenden, Science 267 (1995) 90–93.
[40] M.A. Bianchet, L.A. Seiple, Y.L. Jiang, Y. Ichikawa, L.M. Amzel, J.T. Stivers, Biochemistry 42 (2003) 12455–12460.
[41] L.A. Basso, D.S. Santos, W. Shi, R.H. Furneaux, P.C. Tyler, V.L. Schramm, J.S. Blanchard, Biochemistry 40 (2001) 8196–8203.
[42] A. Fedorov, W. Shi, G. Kicska, E. Fedorov, P.C. Tyler, R.H. Furneaux, J.C. Hanson, G.J. Gainsford, J.Z. Larese, V.L. Schramm, S.C. Almo, Biochemistry 40 (2001) 853–860.
[43] W.P. Jencks, Adv. Enzymol. Relat. Areas Mol. Biol. 43 (1975) 219–410.
[44] M.I. Page, W.P. Jencks, Proc. Natl. Acad. Sci. USA 68 (1971) 1678–1683.
[45] P.M. Legler, M.A. Massiah, A.S. Mildvan, Biochemistry 41 (2002) 10834–10848.
[46] E. Kimura, H. Kitamura, T. Koike, M. Shiro, J. Am. Chem. Soc. 119 (1997) 10909–10919.
[47] C. Thibaudeau, J. Plavec, J. Chattopadhyaya, J. Org. Chem. 61 (1996) 266–286.
[48] N.D. Goldberg, J.L. Dahl, R.E. Parks Jr., J. Biol. Chem. 238 (1963) 3109–3114.
[49] C. Heidelberger, D. Parsons, D.C. Remy, J. Am. Chem. Soc. 84 (1962) 3697–3698.
[50] R.C. Hirt, R.G. Schmitt, H.L. Strauss, J.G. Koren, J. Chem. Eng. Data 6 (1961) 610–612.
[51] A. Piskala, J. Gut, Coll. Czechoslovak Chem. Commun. 26 (1961) 2519–2529.
[52] M.J. Bausch, B. David, P. Dobrowolski, C. Guadalupe-Fasano, R. Gostowski, D. Selmarten, V. Prasad, A. Vaughn, L.H. Wang, J. Org. Chem. 56 (1991) 5643–5651.